INTERNATIONAL JOURNAL OF CLIMATOLOGY
Int. J. Climatol. **29**: 1013–1033 (2009)
Published online 8 October 2008 in Wiley InterScience
(www.interscience.wiley.com) DOI: 10.1002/joc.1742

Dynamics of the Conformal-Cubic Atmospheric Model projected climate-change signal over southern Africa

F. A. Engelbrecht,[a]* J. L. McGregor[b] and C. J. Engelbrecht[a,c]

[a] *Department of Geography, Geoinformatics and Meteorology, University of Pretoria, Pretoria, 0002, South Africa*
[b] *CSIRO Marine and Atmospheric Research, PB1 Aspendale, 3195, Victoria, Australia*
[c] *Agricultural Research Council - Institute for Soil, Climate and Water, Pretoria, PBX79, 0001, South Africa*

ABSTRACT: The projected climate-change signal in simulations by the Conformal-Cubic Atmospheric Model (CCAM) over southern Africa is presented, with particular emphasis on the projected changes in circulation over the region. Current (1975–2005) and future (2070–2100; A2 scenario) climate simulations are used for this purpose.

In the austral winter of the future climate, frontal rain bands are displaced to the south as a result of the subtropical high-pressure belt intensifying to the south of the subcontinent. In spring and autumn, mid- and upper-level highs are simulated to become more prominent over the eastern and central parts of southern Africa. The enhanced subsidence associated with these systems results in generally lower rainfall totals over much of the south-eastern subcontinent. To the north of these highs, enhanced westward moisture advection contributes to increased rainfall totals over northern Mozambique, whilst along the western periphery of the anomalously strong highs, enhanced southward moisture advection results in higher rainfall totals over Namibia, Botswana and the central and western interior of South Africa. In mid-summer, the Indian Ocean High (IOH) is simulated to intensify most over the south-western Indian Ocean (IO). This seemingly results in the more frequent occurrence of the cloud bands that constitute the South Indian Convergence Zone (SICZ) over the south-eastern subcontinent – resulting in generally wetter conditions over this region.

KEY WORDS anthropogenic forcing; climate change; variable-resolution global model; South Indian convergence zone; Indian Ocean High

Received 8 September 2007; Revised 10 April 2008; Accepted 6 June 2008

1. Introduction

Africa is regarded to be one of the continents most vulnerable to anthropogenically induced climate change (e.g. Basher and Briceno, 2005; Meadows, 2006); however, only a small number of climate-change studies have been performed over the continent using high-resolution numerical regional climate models (RCMs) (e.g. Arnell *et al*., 2003; Tadross *et al*., 2005; Olwoch *et al*., 2007). These studies have mostly focused on the projected changes in rainfall and temperature over selected regions. However, RCMs also have the potential to provide insight into how the regional atmospheric circulation may change in response to anthropogenic forcing – which may lead to more clarity on potential future climate change over different regions of the African continent. Although global circulation models (GCMs) may also be used for this purpose, the higher resolution RCMs have the potential to reveal more details of possible changes in the regional circulation (e.g. McGregor, 1997). Having greater understanding of the physical and dynamical mechanisms that drive the projected rainfall changes in a given model simulation may additionally lead to a better evaluation of, and greater confidence in, the projection. In this paper the climate-change signal over southern and tropical Africa as projected by a high-resolution RCM is presented. The emphasis is on analysing the projected changes in dynamic circulation that drive the projected changes in rainfall over southern Africa. Thus the paper strives to gain a deeper understanding of how anthropogenic forcing will modify the regional climate of southern Africa through a change in atmospheric circulation. Southern Africa is taken here as the region bound in the north by latitude 17°S, following Taljaard (1986). The region bounded by 17°S, and the equator will be referred to as 'tropical Africa south of the equator'. A larger area of interest in the study is Africa south of the equator, which will be referred to as the 'subcontinent'.

To obtain the climate-change scenario that is analysed in the paper, simulations of present-day and future climate by an ocean atmosphere general circulation model (OAGCM) were dynamically downscaled over southern and tropical Africa using an RCM. The downscaling was performed by the Conformal-Cubic Atmospheric Model (CCAM), a variable-resolution global model, used here as an RCM. The CCAM and its predecessor, the nested

* Correspondence to: Dr F. A. Engelbrecht, Department of Geography, Geoinformatics and Meteorology, University of Pretoria, Pretoria 0002, South Africa. E-mail: francois.engelbrecht@up.ac.za

limited-area model DARLAM (Division of Atmospheric Research Limited-Area Model), have been used in many regional climate-modelling studies over Australasia and Asia (e.g. McGregor and Walsh, 1994; Walsh and McGregor, 1995; Renwick *et al*., 1999; Whetton *et al*., 2001; Hope *et al*., 2004; Nunez and McGregor, 2007; Lal *et al*., 2008). DARLAM has also been applied to simulate climate and climate change over southern and tropical Africa (Joubert *et al*., 1999; Engelbrecht *et al*., 2002; Olwoch *et al*., 2007). In this study, CCAM is used to simulate climate for the periods 1975–2005 and 2070–2100. Lower boundary forcing was obtained from the Commonwealth Scientific and Industrial Research Organization (CSIRO) Mk3.0 OAGCM, which was integrated for the period 1871–2100 with increasing greenhouse gas concentrations according to the A2 Special Report on Emissions Scenarios (SRES) scenario. The CCAM simulations were performed as part of a project that investigated the hydrological impacts of climate change over southern Africa (Engelbrecht, 2005; Schulze *et al*., 2005). Here the simulations are analysed from a dynamic perspective, in order to gain deeper understanding of the physical mechanisms behind the projected changes in rainfall.

The RCM simulations presented here, having a horizontal resolution of about 0.5°, provide the highest resolution climate-change projections ever obtained over the southern African region for an extended simulation period. In fact, only a small number of regional climate-change scenarios have been derived to date for southern Africa. Tadross *et al*. (2005) used two RCMs (the 5th generation PSU/NCAR mesoscale model, MM5) and the 'Providing REgional Climates for Impact Studies' model (PRECIS, of the Hadley Centre, UK) to downscale 10 years of control and 10 years of future southern African climate, as simulated by the HadAM3 GCM under the A2 SRES scenario. For the relatively short periods simulated, the two models indicated broadly consistent changes for the subcontinent as a whole (Tadross *et al*., 2005). For the period October–December the models simulated drier conditions over the tropical western side of the subcontinent in the future climate, with MM5 extending the drier conditions further south into southern Namibia and the Northern Cape in South Africa. For the period January–March, drier conditions were simulated in the west towards the tropics, with wetter conditions towards the east. Mid-summer and mid-winter climate for two 10-year periods of present-day and future conditions (A2 SRES scenario) were simulated using DARLAM nested within the CSIRO Mk2 GCM by Olwoch *et al*. (2007). For the future climate, the model simulated generally drier conditions over South Africa in winter, due to a displacement of frontal rainbands towards the south. For mid-summer the model simulated wetter conditions over the western to central interior of South Africa.

An empirical technique based on self-organizing maps (SOMs) was used to downscale climate-change projections from three GCMs for December to February (DJF) and June to August (JJA) by Hewitson and Crane (2006). They predicted that South Africa will experience increased summer rainfall over the convective rainfall region of the central and eastern plateau, with an even larger increase over and to the east of the eastern escarpment. The south-western Cape is projected to experience little change, with slight drying in summer and a slight decrease in wintertime frontal rainfall. An important feature of their work is that the downscaled scenarios obtained from different GCMs are spatially coherent with respect to the patterns of the projected regional rainfall changes, although the magnitudes of the different downscaled projected changes differed considerably. The results of Tadross *et al*. (2005) and Hewitson and Crane (2006) have given rise to the perception that South Africa will become wetter in the east and drier in the west in response to enhanced greenhouse gas forcing (e.g. Department of Environmental Affairs and Tourism (DEAT), 2006; Meadows, 2006). More work is required to investigate the validity of this perception, given all the uncertainties associated with projections of climate change (e.g. Hulme *et al*., 2005; Christensen *et al*., 2007). In particular, gaining insight into how the regional circulation may be expected to change in response to anthropogenic forcing may help distinguish between plausible and less plausible projections of changes in rainfall patterns over southern Africa.

The ability of CCAM to simulate the intra-annual rainfall and circulation cycle over the subcontinent is verified against observations before the simulation of climate change is presented. The main purpose of this paper, however, is to describe the projected climate-change signal in the rainfall distribution over the subcontinent and then to draw attention to features of the anomalous atmospheric circulation which probably contribute to these changes. Indeed the projected changes in rainfall are shown to have plausible physical and dynamical causes that may be linked to some of the main known modes of climate variability over the region. Still, it should be borne in mind that the results presented here are from a single estimate of possible climate change over tropical and southern Africa. Because of the uncertainties that still exist in representing the ocean-atmosphere-landmass system in GCMs and RCMs (e.g. Hulme *et al*., 2005; Christensen *et al*., 2007), it is desirable to assess the outputs from a range of models integrated according to different SRES scenarios, in order to estimate the likely range of possible outcomes of future climate. The study may be seen as providing a member of such an ensemble of projections. The paper is organized as follows: Section 2 outlines the model description and experimental configuration. In Section 3 the present-day simulated intra-annual rainfall and circulation climatology is compared against observations at the synoptic-scale. The simulated future climate is presented and discussed in Section 4, with special emphasis on linking the projected change in rainfall over southern Africa with changes in dynamic circulation. A summary and conclusions can be found in Section 5.

DOI: 10.1002/joc

2. The conformal-cubic atmospheric model and experimental configuration

CCAM is a GCM which may be used in variable-resolution mode to function as an RCM. That is, the model may be integrated with high horizontal resolution over the area of interest, with the resolution gradually decreasing as one moves away from the area of interest. Compared to the more traditional nested limited-area modelling approach (e.g. McGregor, 1997), variable-resolution modelling provides great flexibility for dynamic downscaling from any global model, essentially requiring only sea-surface temperatures and, optionally, far-field winds from the host model (McGregor and Dix, 2001; Wang *et al*., 2004). It also avoids other problems that may occur with limited-area models, such as reflections at lateral boundaries. CCAM is formulated on a quasi-uniform grid, derived by projecting the panels of a cube onto the surface of the Earth. The model can be run in either stretched mode for variable-resolution regional modelling, or in a non-stretched mode to provide quasi-uniform resolution globally.

CCAM employs a two-time-level semi-implicit hydrostatic formulation. Semi-Lagrangian horizontal advection with bi-cubic spatial interpolation is used (McGregor, 1996), with total-variation-diminishing vertical advection. The model uses an unstaggered grid, with winds transformed reversibly to/from C-staggered locations before/after gravity wave calculations (McGregor, 2005a). More details on the geometrical aspects and dynamical features of CCAM can be found in McGregor (2005b). The model employs a wide range of physical parameterizations. These include a CSIRO mass-flux cumulus convection scheme, which includes downdrafts and the evaporation of rainfall. The GFDL parameterization (Schwarzkopf and Fels, 1991) for long-wave and short-wave radiation is used, with interactive cloud distributions diagnosed from liquid and ice-water content (Rotstayn, 1997). Gravity wave drag is also parameterized. A stability-dependent boundary layer is used, with non-local vertical mixing. The model also includes a canopy scheme, with six layers for soil temperatures (Gordon *et al*., 2002), six layers for soil moisture solved using Richard's equation, and three layers of snow.

For the CCAM regional climate simulations presented here, a C64 set-up ($6 \times 64 \times 64$ grid points) was used, with 18 pressure-sigma levels in the vertical. A modest Schmidt stretching factor of 2.5 was used, giving a resolution of about 60 km over southern Africa. The stretched conformal-cubic grid over southern and tropical Africa is shown in Figure 1. Initial conditions and sea-surface temperatures (SSTs) were provided from a transient 1871–2100 simulation of the CSIRO Mk3.0 AOGCM. In both the CSIRO Mk3.0 AOGCM and CCAM, observed greenhouse gas concentrations were used in simulations for the years between 1871 and 2000, whilst concentrations predicted according to the A2 SRES scenario were used to force the models for simulation years between 2001 and 2100. Both models also include the direct effect from estimated increases in aerosol concentrations during the period. Stratospheric ozone concentrations, either observed or estimated, were provided for each month of the simulation.

In similar climate-change experiments over the Australian region, a more strongly stretched version (Schmidt factor of 3.3) has been used (e.g. McGregor *et al*.,

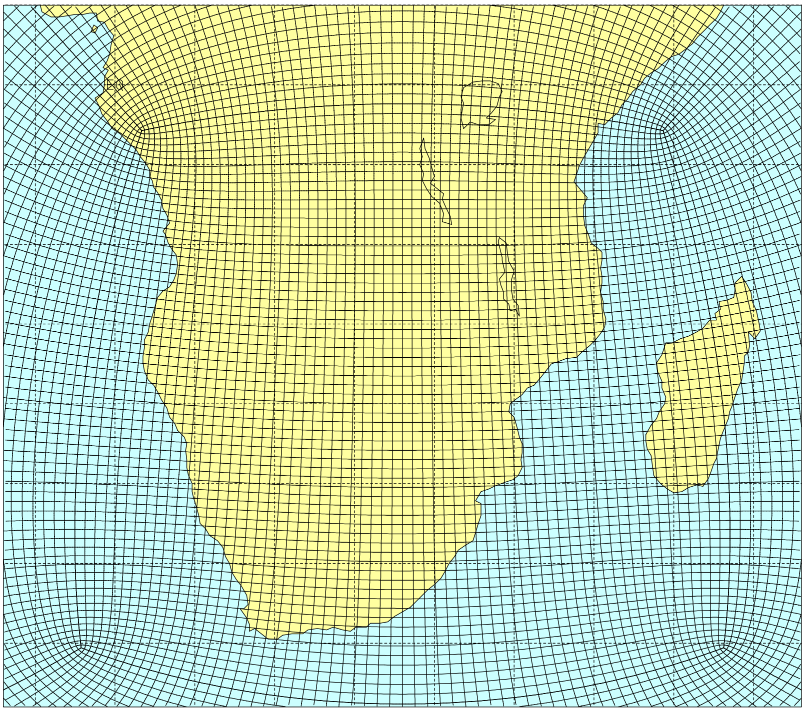

Figure 1. The modestly stretched conformal-cubic grid over southern and tropical Africa. This figure is available in colour online at www.interscience.wiley.com/ijoc

2002) with a C48 grid having fewer grid points. That configuration also had a resolution of about 60 km over the area of interest, but the far-field region gets as coarse as 700 km. For those runs, it was considered prudent to employ a far-field wind-nudging technique, to compensate for the coarseness of the grid in the far field. It was considered that nudging was not required for the present simulations, as the grid stretching is less strong, and the coarsest far-field resolution is only about 450 km. Similarly, Deque *et al.* (1998) chose not to use far-field nudging for their modestly stretched global simulations.

3. CCAM simulations of the present-day intra-annual rainfall cycle over the subcontinent

A necessary condition for confidence in a model projection of climate change is that the model should be able to adequately simulate present-day climate, since the ability to predict future climate depends partly on the model's ability to simulate current climate (Sushama *et al.*, 2006). The long-term mean circulation patterns and surface fields should be well simulated, and also the variability on many time scales from diurnal through seasonal to decadal and beyond (Battisti, 1995; Renwick *et al.*, 1999). Thus, full validation of a simulation against observations is an extensive task. Here the ability of CCAM to simulate yearly rainfall totals and the intra-annual rainfall cycle over the subcontinent is qualitatively verified against observations before the simulation of climate change is presented. The observed and simulated seasonal cycles in the 850 and 500 hPa geopotential height over the region are also presented, and linked to the corresponding observed and simulated rainfall cycles. For the purpose of pointing out regional features in the rainfall cycle, the subcontinent is divided into a number of subregions (Figure 2). The subregions are the south-western Cape of South Africa (region A), the Cape south coast of South Africa (region B), the east coast and eastern interior of South Africa (region C), the western subcontinent (region D), the central subcontinent (region E), north-eastern South Africa, southern Zimbabwe and southern Mozambique (region F), northern Mozambique and Tanzania (region G), Kenya and Uganda (East Africa, region H), the northern subcontinent (region I) and the subtropical subcontinent (region J). The precise longitudinal and latitudinal boundaries of the various regions selected are shown in Table I.

The observed rainfall climatology was obtained from the Climatic Research Unit (CRU) for the period 1960–1990 (New *et al.*, 1999). Many of the spatial and temporal characteristics of a range of surface climate variables over southern and tropical Africa can be observed in the CRU data (Engelbrecht *et al.*, 2002). Figure 3 shows the rainfall totals over the subcontinent for CRU and the CCAM simulation. Many of the regional features of the observed rainfall pattern over southern Africa are captured in the model simulation. These include the west–east gradient in rainfall totals over South Africa and the band of relatively low rainfall that stretches from Namibia in the west over Botswana to Zimbabwe and north-eastern South Africa in the east. However, the model generally overestimates rainfall totals over southern Africa, most prominently over and to the east of the eastern escarpment of South Africa. The simulation of rainfall totals over the latter region is known to be problematic for RCMs (e.g. Engelbrecht *et al.*, 2002; Christensen *et al.*, 2007). Over tropical Africa south of the equator, the model correctly simulates relatively low rainfall over the eastern parts of Tanzania and Kenya, with rainfall increasing to the west over the Great

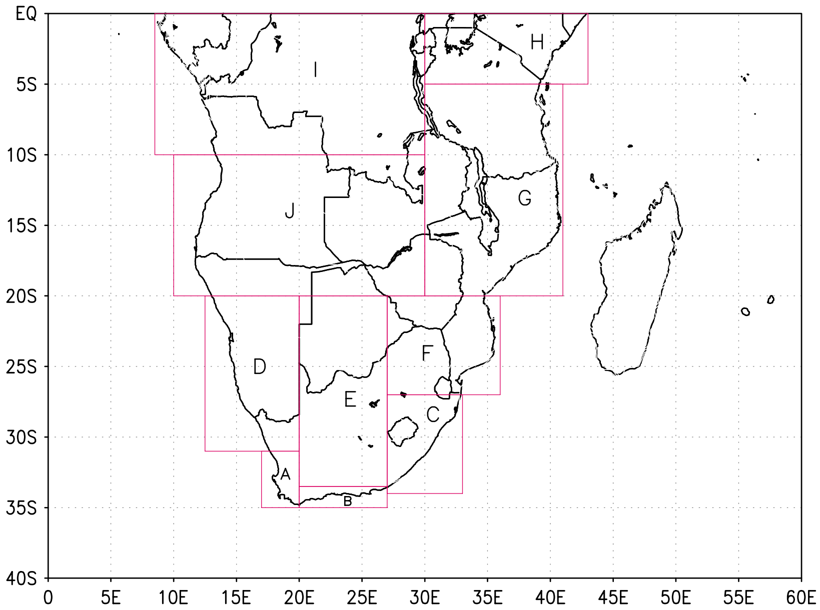

Figure 2. Locations of the different subregions covering the subcontinent. This figure is available in colour online at www.interscience.wiley.com/ijoc

Table I. Locations of subregions covering the subcontinent.

	Region	Latitude	Longitude
A	South-western Cape	$-35^\circ < \phi \leq -31^\circ$	$17^\circ < \lambda \leq 20^\circ$
B	Cape south coast	$-35^\circ < \phi \leq -33.5^\circ$	$20^\circ < \lambda \leq 27^\circ$
C	Eastern South Africa	$-34^\circ < \phi \leq -27^\circ$	$27^\circ < \lambda \leq 33^\circ$
D	Western subcontinent	$-31^\circ < \phi \leq -20^\circ$	$12.5^\circ < \lambda \leq 20^\circ$
E	Central subcontinent	$-33.5^\circ < \phi \leq -20^\circ$	$20^\circ < \lambda \leq 27^\circ$
F	North-eastern South Africa, S Zimbabwe and S Mozambique	$-27^\circ < \phi \leq -20^\circ$	$27^\circ < \lambda \leq 36^\circ$
G	N Mozambique and Tanzania	$-20^\circ < \phi \leq -5^\circ$	$30^\circ \leq \lambda \leq 41^\circ$
H	East Africa	$-5^\circ < \phi \leq -0^\circ$	$30^\circ \leq \lambda \leq 43^\circ$
I	Northern subcontinent	$-10^\circ < \phi \leq -0^\circ$	$8.5^\circ \leq \lambda < 30^\circ$
J	Subtropical subcontinent	$-20^\circ < \phi \leq -10^\circ$	$10^\circ < \lambda < 30^\circ$

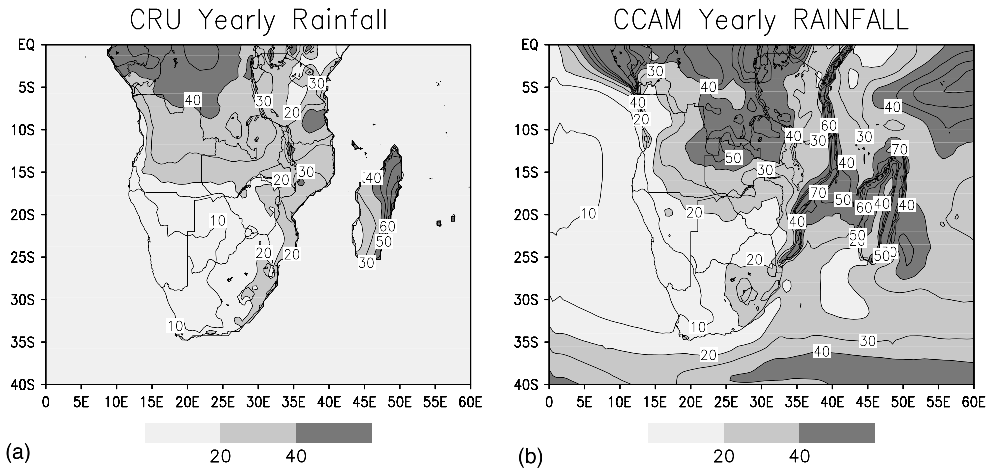

Figure 3. CRU-observed (a) and CCAM-simulated (b) yearly rainfall totals in (mm/day)*10 over the subcontinent.

Lakes region and the northern Democratic Republic of Congo (DRC). However, the model overestimates rainfall totals rather severely over the southern DRC, northern Zambia, western Tanzania and the Mozambiquen coastline.

3.1. CCAM simulations of the seasonal rainfall and circulation cycles

The seasonal rainfall and circulation cycles over the subcontinent are depicted in Figures 4 and 5, respectively. Because seasonal rainfall varies greatly over the subcontinent, the observed (CRU data) and simulated seasonal rainfalls are expressed as a percentage of the respective annual totals. Figure 4 shows the observed and simulated seasonal rainfall percentages for JJA, September to November (SON), DJF and March to May (MAM). Figure 5 shows the corresponding seasonal circulation anomalies (relative to the annual mean), at the 850 hPa (contours) and 500 hPa (shaded) levels. The observed seasonal circulation anomalies are long-term (1975–2005) averages, obtained from the National Centers for Environmental Prediction (NCEP) reanalysis data (Kalnay *et al.*, 1996).

During the austral winter (JJA), circulation over southern Africa is largely dominated by the intense subtropical high-pressure belt (e.g. Preston-Whyte and Tyson, 1988; Taljaard, 1996). Anomalously high values of geopotential occur in the lower troposphere, in particular over the central and southern subcontinent (note the distribution of the 850 hPa contours in Figure 5(a)). In the subsident conditions that prevail, most of the subcontinent's interior receives a small portion (less than 5%) of its annual rainfall (Figure 4(a); Taljaard, 1986). However, the winter rainfall region of South Africa (the south-western Cape, region A) receives the bulk of its annual rainfall (about 30–50%) from frontal systems during these three months (e.g. Preston–Whyte and Tyson, 1988; Taljaard, 1996; Reason and Rouault, 2002). The Cape south coast of South Africa (region B), a narrow round-the-year rainfall region, receives up to 30% of its annual rainfall during JJA. Note that the negative 850 hPa geopotential anomalies to the south-west of the subcontinent (Figure 5(a)) indicate the eastward passage of mid-latitude cyclones to the south of the subcontinent during JJA (e.g. Taljaard, 1967). It may also be noted that although tropical Africa south of the equator is relatively dry in JJA compared to other seasons, the extreme northern parts receive up to 15–20% of their annual rainfall due to rainfall that occurs at the southern boundary of the Inter-Tropical Convergence Zone (ITCZ). Comparing Figure 4(e) to (a), it may be seen that CCAM simulates the regional distribution of rainfall percentages during JJA very well. Important features simulated correctly by the model are the generally dry conditions over the subcontinent, relatively

DOI: 10.1002/joc

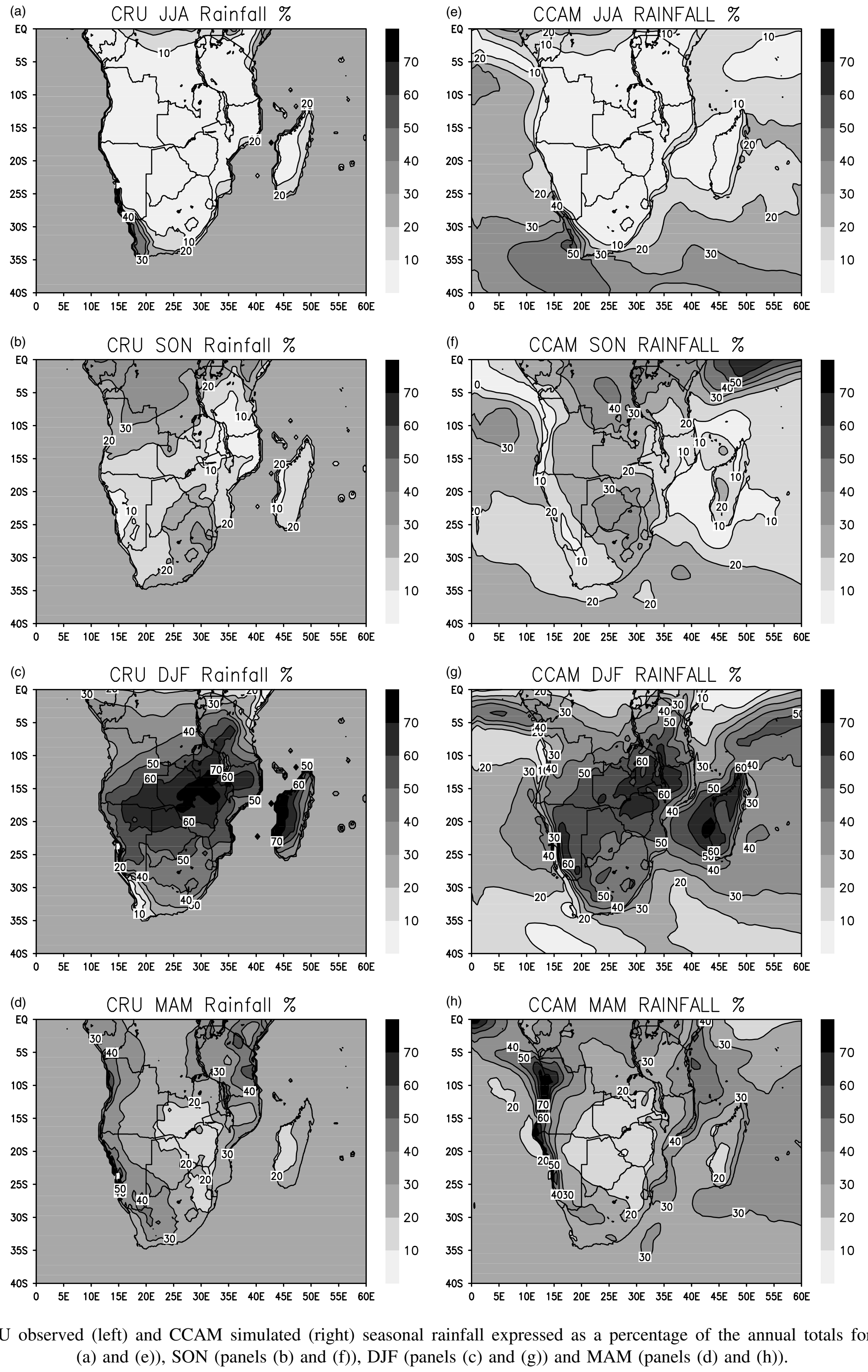

Figure 4. CRU observed (left) and CCAM simulated (right) seasonal rainfall expressed as a percentage of the annual totals for JJA (panels (a) and (e)), SON (panels (b) and (f)), DJF (panels (c) and (g)) and MAM (panels (d) and (h)).

wet conditions over tropical Africa south of the equator, relatively wet conditions along the Mozambiquen coast (compared to areas further inland) and the high rainfall percentages over the south-western Cape and Cape south coast of South Africa. Indeed the model correctly simulates anomalously high geopotential over the subcontinent (Figure 5(e)). It may also be noted that the model correctly simulates the presence of a frontal rainband south of the subcontinent for JJA (Figure 4(e), not shown in Figure 4(a)). However, the model simulates

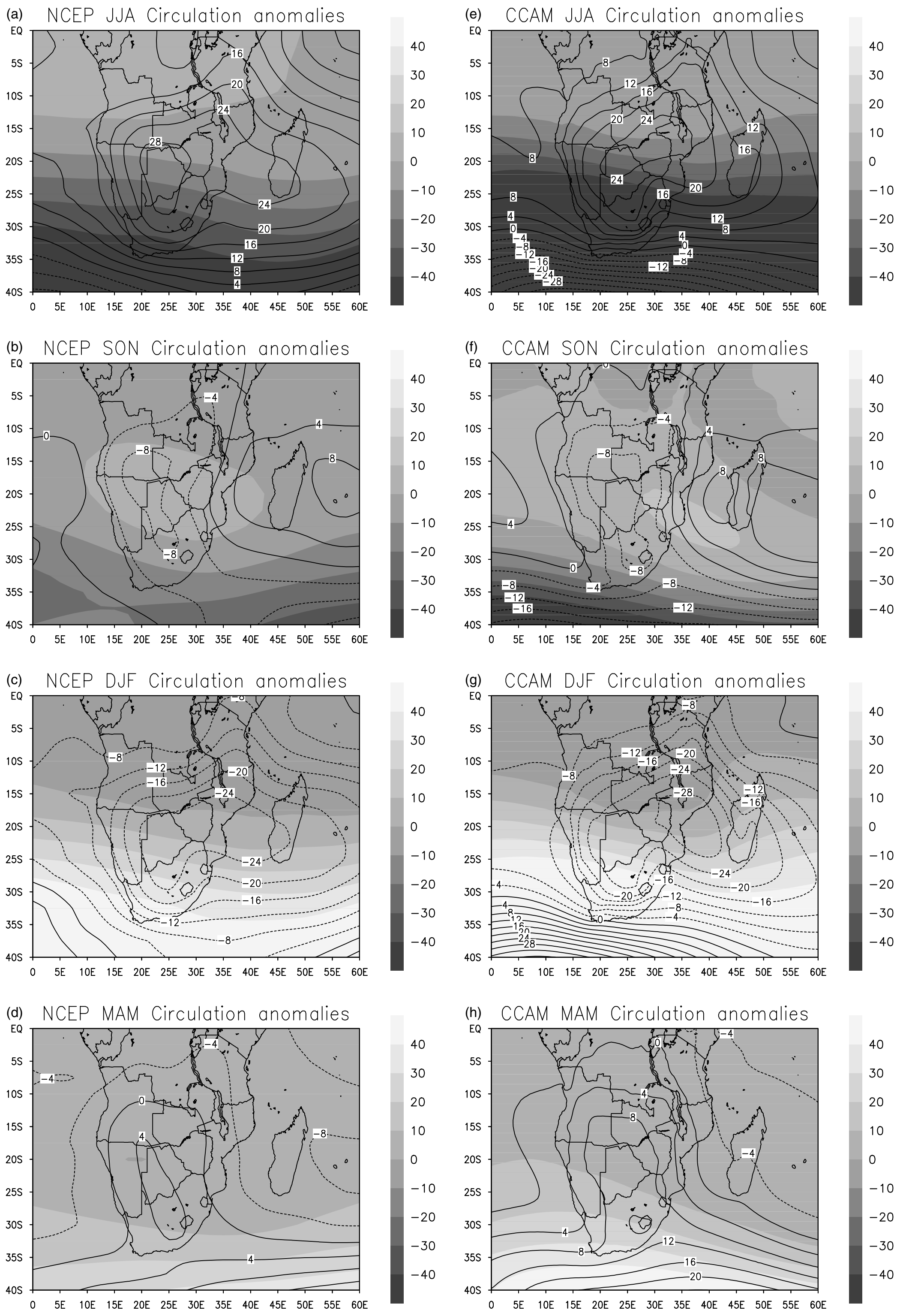

Figure 5. NCEP reanalysis (left) and CCAM simulated (right) seasonal circulation anomalies at the 850 hPa (contours) and 500 hPa (shaded) levels for JJA (panels (a) and (e)), SON (panels (b) and (f)), DJF (panels (c) and (g)) and MAM (panels (d) and (h)). Anomalies are calculated relative to the respective annual long-term means and are given in geopotential meters (gpm).

too strong negative 850 hPa geopotential anomalies to the south of the country, which may be indicative of exaggerated cyclonic activity in the simulation. Correspondingly, when comparing the simulated (Figure 5(e)) and observed (Figure 5(a)) 500 hPa geopotential height anomalies, it may be noted that the model simulates too low 500 hPa heights for JJA, particularly over the southern part of the domain. This suggests that the model has a cold tropospheric bias in winter (through the hypsometric equation).

Anomalously low geopotential height develops over the central subcontinent in the lower troposphere during SON, as the continental trough deepens in response to enhanced solar heating (Figure 5(b)). An associated rise in the 500 hPa height occurs over the central subcontinent. The solar heating and associated southward movement of the ITCZ breaks the winter pattern of subsidence. Kenya, the DRC and northern Angola receive 30–40% of their annual rainfall (Figure 4(b)). The east coast and eastern interior of South Africa similarly receive 30–40% of their annual rainfall during spring. The remainder of the subcontinent remains relatively dry during SON, receiving less than 20% of the annual rainfall during this period. Over the winter rainfall region, rainfall decreases significantly with respect to winter months, with region A receiving about 20% of the annual total rainfall during SON. CCAM correctly simulates high rainfall percentages over the northern DRC, Kenya and northern Angola during SON (Figure 4(f)). The model satisfactorily captures the high SON rainfall percentages over the east coast and eastern interior of South Africa. However, in the simulation a band of spuriously high rainfall percentages links the high rainfall percentage regions C and J. It seems as if the model simulates too strong a link between the ITCZ and southern Africa. Rainfall percentages are overestimated over the central subcontinent (region E), in particular. From the simulated SON circulation anomalies (Figure 5(f)), it can be seen that the model satisfactorily captures the observed strengthening of the continental trough and rise in 500 hPa geopotential height over the central subcontinent. The model also simulates anomalously high geopotential heights in the lower troposphere over the Indian Ocean (IO), a feature that is also present in the observed SON circulation anomalies (Figure 5(b)). However, the model overestimates the increase in geopotential over the IO and as a result the zonal geopotential gradient between the IO and the central subcontinent is also overestimated. This feature of the model simulation is favourable for enhanced southward moisture advection over the subcontinent, which may explain the band of spuriously high rainfall totals simulated over the central interior. The relatively low rainfall that occurs over the far western subcontinent (Figure 4(b)) is simulated well (Figure 4(f)), and so are the lower rainfall percentages that occur over region A with respect to JJA.

The most prominent feature of the observed DJF rainfall is that the highest rainfall percentages and totals occur in a zonal band stretching from northern Namibia in the west to northern Mozambique and southern Tanzania in the east (Figure 4(c); e.g. Engelbrecht *et al.*, 2002). Much of the central and subtropical subcontinent receives more than 60% of its annual rainfall during DJF. The zonal band of high rainfall percentages indicates the average position of the ITCZ during these months, and is associated with anomalously low geopotential in the lower troposphere (Figure 5(c)). To the south of the zonal band of high rainfall, a well-defined west–east directed gradient in rainfall totals occurs over South Africa (not shown). It may also be noted that there is a pattern of high rainfall percentages and totals extending from northern Namibia to the south. The model simulates the basic features of the DJF rainfall pattern satisfactorily (Figure 4(g)). The zonal band of high rainfall over the central and subtropical subcontinent is captured in the simulation, as well as the associated band of anomalously low 850 hPa geopotential heights (Figure 5(g)). The model also correctly indicates relatively drier conditions over the northern subcontinent during DJF. The west–east gradient in rainfall totals over South Africa during DJF (not shown) is captured in the model simulation, as well as the observed pattern of high rainfall percentages and totals extending from northern Namibia to the south. However, the model spuriously simulates this pattern to extend into the western interior of South Africa.

During MAM, geopotential height becomes anomalously high in the lower troposphere over southern Africa (Figure 5(d)), and increasingly subsident conditions set in over the subcontinent. The zonal band of high rainfall percentages that was present over the central subcontinent during DJF is displaced to the northern subcontinent during MAM (Figure 4(d)), in association with the northward moving ITCZ. Rainfall decreases significantly over the eastern parts of southern Africa with respect to the DJF period. Another prominent feature of the MAM rainfall pattern is the high percentage of rainfall that falls over Namibia and the western interior of South Africa. Much of the western subcontinent receives more than 30% of its annual rainfall during MAM. This interesting feature has been attributed to the positioning of the continental trough and the high frequency of occurrence of cut-off lows over the western parts of southern Africa during these months (Taljaard, 1986); Figure 5(d) reveals that this feature occurs to the west of the region of maximum positive MAM 850 hPa height anomalies. These positive anomalies are representative of the weakening and northwestward shift of the continental trough that occurs in MAM. It may be noted that a west–east directed gradient in rainfall totals still exists over South Africa during MAM (not shown), although the gradient in rainfall percentages is directed from east to west. The model captures the MAM rainfall pattern remarkably well (Figure 4(h)). Prominent features such as the relatively drier conditions over the eastern subcontinent, the zonal band of high rainfall over the northern subcontinent and the high rainfall percentages over the western subcontinent are all present in the model simulation. The model correctly portrays the pattern of increasing geopotential over southern Africa in MAM at 850 hPa (Figure 5(h)); however, it overestimates the strength of the anomaly. Seemingly correspondingly, the model somewhat overestimates the occurrence of relatively drier conditions over the eastern subcontinent; also the occurrence of high rainfall percentages over the western interior of South Africa is confined to regions a little further to the west than is observed.

3.2. CCAM simulations of the intra-annual rainfall variability over different subregions

The modelled monthly rainfall totals over various subregions of the subcontinent are finally compared to the corresponding observed totals. The graphs for the different regions allow a comparison between how the model simulates month-to-month changes in the rainfall and the corresponding observed changes. The curves in Figure 6 represent monthly rainfall totals. Curves obtained from displaying monthly percentages of the mean annual rainfall for the various regions (not shown) are very similar to the curves displayed in Figure 6. Note that only CCAM grid points over the subcontinent were used in calculating the monthly rainfall values for each region, in correspondence to the nature of the land-based CRU data.

Region A is a winter rainfall region with the onset of the rainy season occurring in April and ending in September (Figure 6(a); e.g. Taljaard, 1986). Interesting features of the intra-annual rainfall cycle over this region are that the rainfall peaks in June rather than July, and that rainfall in July is also lower than in August (Figure 6(a); also see Taljaard, 1986). CCAM simulates the intra-annual rainfall cycle over region A well and captures the occurrence of the rainfall peak in June. However, the model simulates a slight decrease in rainfall in August compared to July, instead of the moderate increase that is observed. The model generally underestimates rainfall totals over region A, particularly for the months April to June.

The Cape south coast of South Africa (region B) is an all-season rainfall area. The monthly variations in rainfall over this region hardly exceed 10% of the normal at any time (e.g. Taljaard, 1986), although two maxima (in April and August) and a period of minimum monthly totals (December and January) can be discerned in the CRU data (Figure 6(b)). Region B is the region where the model fares the poorest in simulating the intra-annual rainfall cycle. Although the model correctly simulates minimum rainfall in January and a rising tendency in monthly totals during February and March, it fails to simulate the observed rainfall maxima that occur in April and August (Figure 6(b)). In fact, the model generally underestimates rainfall over region B, particularly in April and during August to November.

The east coast and eastern interior of South Africa (region C) is a summer rainfall region. The onset of the rainy season occurs in September and it ends in April (Figure 6(c)). The December rainfall total is slightly less than the November total and the monthly rainfall maximum occurs in January. CCAM simulates the intra-annual rainfall cycle over the region satisfactorily, although it somewhat overestimates the monthly rainfall totals (Figure 6(c)). The model also fails to capture the slight decrease in the December totals compared to November, and instead simulates rapidly rising rainfall from November to December.

Region D (the western subcontinent) is a summer rainfall region with a well-defined late-summer rainfall maximum (Figure 6(d)). Very dry conditions prevail from May to September, with the onset of rainfall occurring in October. However, rainfall totals remain relatively low during the early summer, reaching values of about 0.4 mm/day during November and December. A pronounced increase in rainfall occurs in January, with the monthly rainfall peaking in February at about 1.4 mm/day. Rainfall totals remain relatively high in March, and interestingly the April total is higher than the December total (e.g. Taljaard, 1986). It may be noted that Taljaard (1986) has linked the late-summer rainfall maximum over Namibia and western South Africa to the positioning of the continental trough and the high frequency of cut-off lows that occur over the region in the late summer. The model simulates the January–April rainfall totals over region D well and correctly indicates that the rainfall maximum occurs in February (Figure 6(d)). The model also correctly simulates the dry conditions that prevail from May to September and the onset of rainfall in October, but slightly overestimates the monthly totals for this period. For November and December the overestimation of rainfall totals by the model is more severe, and the model incorrectly indicates more rainfall for these two months than for April.

Region E (the central subcontinent) is a summer rainfall region with an intra-annual cycle in rainfall (Figure 6(e)) similar to that of the adjacent region D. However, the late summer (February) rainfall peak is less well pronounced than in region D, and region E is generally wetter than region D. CCAM simulates the intra-annual rainfall cycle over region E satisfactorily. However, the model overestimates the February and December rainfall totals rather severely, by as much as 1.5 mm/day.

Region F (north-eastern South Africa, southern Zimbabwe and southern Mozambique) is another summer rainfall region. The winter is very dry whereafter rainfall increases slightly in September (Figure 6(f)). The monthly rainfall rises more rapidly from October onwards and peaks in February, whereafter rainfall decreases rapidly towards the winter minimum. CCAM satisfactorily simulates the intra-annual rainfall cycle over the region, and correctly indicates that the rainfall maximum occurs in February (rather than in January as is the case over region C in the south). However, the model generally overestimates rainfall over region F, with the overestimation being rather severe (about 1.8 mm/day) for February.

Region G (northern Mozambique and Tanzania) is another well-defined summer rainfall region. The months July–September are relatively dry with the rainy season starting in October (Figure 6(g)). Rainfall rises rapidly during November and peaks from December to March, whereafter the monthly totals decline rapidly during April and May. CCAM gives a satisfactory simulation of the intra-annual rainfall cycle over this region. However, it spuriously indicates December to be the month of maximum rainfall, instead of February as observed. In fact, the December rainfall total over the region is overestimated by about 2 mm/day. Rainfall totals are also

DOI: 10.1002/joc

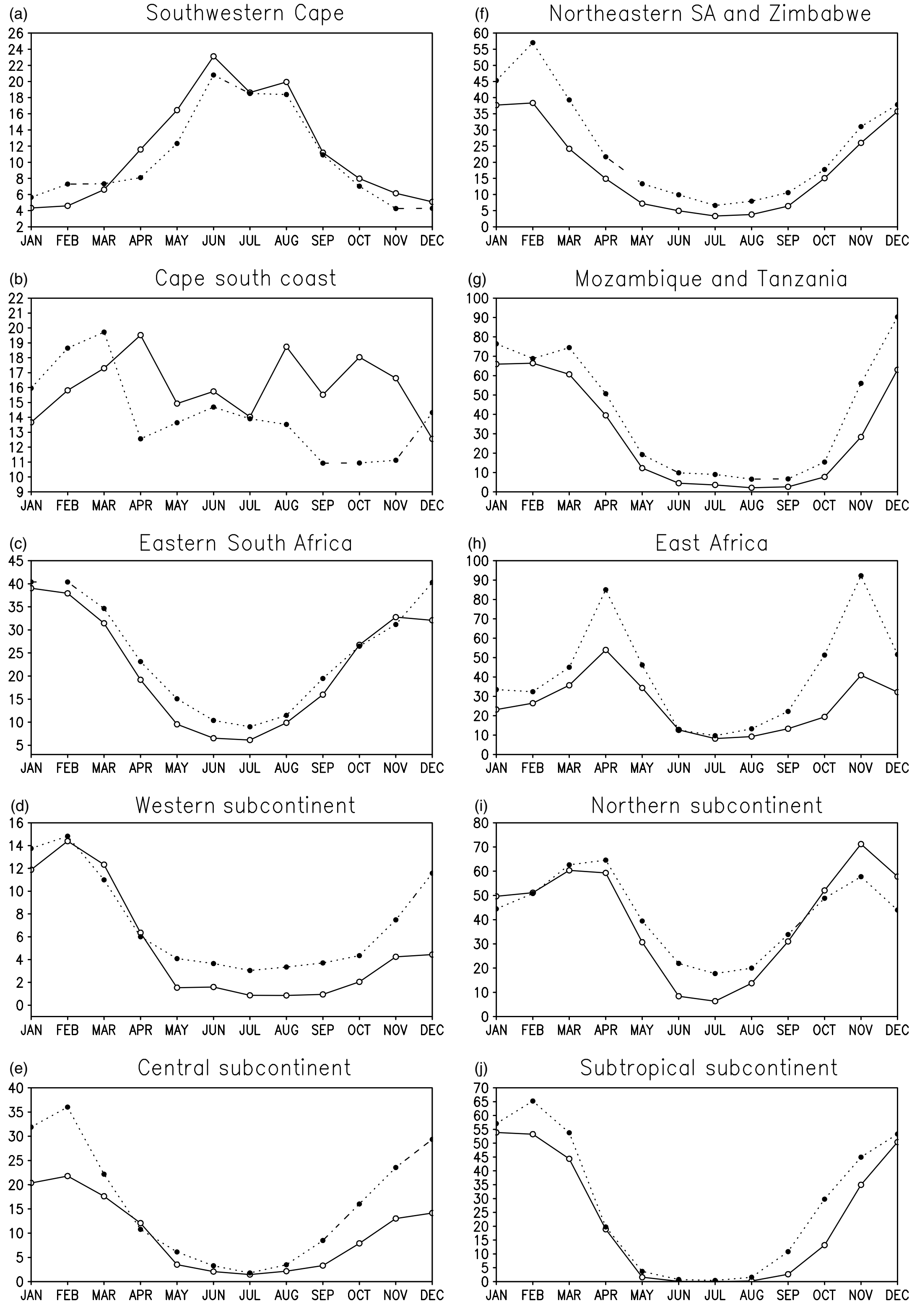

Figure 6. CRU observed (solid lines) and CCAM simulated (dotted lines) monthly rainfall totals (mm/day)*10 over different regions of the subcontinent.

overestimated for the other months, but less severely than the December total.

East Africa (region H) displays an interesting intra-annual cycle in rainfall, with maxima in the monthly rainfall totals occurring in April and November (Figure 6(h)). The maxima occur in association with the southward and northward pass of the ITCZ over the region during November and April, respectively. The formation of the East African jet stream also contributes to the autumn and spring rainfall maxima. CCAM correctly simulates the occurrence of the two rainfall maxima, but spuriously indicates the November maximum to be higher

DOI: 10.1002/joc

than the April maximum. The model severely overestimates rainfall over the region during these two months, by about 4 mm/day during April and 5 mm/day during November.

The intra-annual cycle of rainfall over region I (the southern Congo, DRC, and far northern Angola) is likewise largely determined by the meridional displacements of the ITCZ. A clear rainfall minimum occurs from June to August, when the ITCZ reaches extreme northern locations (Figure 6(i)). The monthly rainfall increases rapidly in September and October as the ITCZ starts to advance southwards. Rainfall maxima occur in November and again in March–April, in association with the southward and northward pass of the ITCZ, respectively. The monthly rainfall remains relatively high between December and February and during May as the ITCZ lurks to the south and north of the region, respectively. The highest monthly rainfall (almost 7 mm/day) occurs in November. CCAM correctly simulates the timing of the rainfall maxima and minimum. However, it incorrectly simulates lower rainfall for November compared to March and April. The model generally simulates rainfall totals over this high rainfall region fairly accurately. However, it simulates too wet conditions during July (an overestimate of about 1 mm/day) whilst it underestimates the November maximum by about 1 mm/day.

Region J is a summer rainfall region that experiences almost rainless winters in the subsident conditions that prevail over the subtropical subcontinent from May to August (Figure 6(j)). The onset of the rainy season is in September when the ITCZ starts its southward march. From October onwards there are rapid rises in the monthly rainfall totals, with the rainfall peaking in January and February (at more than 5 mm/day) when the ITCZ is located within the region. Rainfall remains relatively high in March but decreases rapidly during April as the ITCZ moves into the northern hemisphere. CCAM simulates the intra-annual rainfall cycle over this region satisfactorily, although it erroneously indicates a pronounced February rainfall maximum. The monthly rainfalls are generally overestimated over this region, with the overestimation most severe during February (by about 1.2 mm/day) and October (by about 1.6 mm/day).

From the preceding discussion it may be seen that the areas with highest seasonal rainfall percentages follow an almost circular path over southern Africa between SON and MAM (e.g. Taljaard, 1986). Starting out along the east coast and the adjacent interior of South Africa in SON, the areas with most rapidly increasing rainfall percentages are being successively displaced to north-eastern South Africa, Zimbabwe, Zambia, northern Botswana and northern Namibia, western and southern Namibia and ending over the western interior of South Africa in MAM (note that the regions of largest rainfall percentages are not necessarily also the regions of highest local rainfall totals). Some of the circulation features responsible for these features are discussed by Taljaard (1986). Although a number of shortcomings in the model simulation have been identified, it may be said that CCAM generally simulates the regional rainfall and circulation cycle over southern Africa remarkably well, giving some confidence in its projections of future rainfall. A more detailed verification of the model simulation of present-day climate, based on daily rainfall and circulation statistics, falls beyond the scope of this paper. Some more details on how CCAM simulates present-day temperature patterns and daily rainfall statistics over southern Africa may be found in Engelbrecht (2005) and Schulze *et al.* (2005).

4. Simulations of climate change

The climate-change signal is defined as the difference between the simulated climates under future and current forcings. This definition is based on the assumption that systematic errors (biases) in the model simulations will partially cancel when subtracting the current and future simulations. See Sushama *et al.* (2006) for the shortcomings of this definition. Considering changes in the simulated climatological means under future and current forcings provides a direct measure of systematic change in climate, and is perhaps the most fundamental way of defining the climate-change signal. The differences between the simulated future and present-day climates are considered for rainfall (expressed as a percentage change), 1000, 850, 500, and 200 hPa geopotential height (gpm) and the vertically integrated zonal and meridional moisture flux (m s^{-1} kg/kg) for each of the four seasons in Figures 7–10. The Wilcoxon–Mann–Whitney rank-sum test was used to test if the corresponding present-day and future seasonal rainfall climatologies differ in location, and the result for each season is also displayed in the mentioned figures.

To enhance interpretation of changes in the seasonal climatological means, changing frequency of occurrence of high and low pressure systems over the subcontinent was also investigated. For this purpose, the study area was divided into $5^\circ \times 5^\circ$ degree grid boxes, and the average geopotential over each grid box was calculated – in 12-hourly intervals covering the 62-year period under investigation. For each of these time-intervals, the grid boxes that were local maxima (indicative of the presence of synoptic-scale high-pressure cells or ridges) or minima (indicative of the presence of local low pressure cells or troughs) of geopotential were identified. The seasonal change in the frequency of occurrence of local geopotential maxima, calculated for each grid box over 12-hourly intervals, is presented in Figure 11 for the 850 and 500 hPa levels. This analysis gives additional insight into the change of behaviour of synoptic-scale lows and highs in the present-day and future climates. A more extensive analysis of changes in synoptic-scale circulation at the daily time-scales, and analysis of changes in the frequency of rain days and rainfall intensity may additionally be performed. However, here the emphasis is on analysing how systematic changes in circulation relate to the rainfall climate-change signal. A more extensive analysis of change in circulation and rainfall at the daily time scale falls beyond the scope of the paper.

DOI: 10.1002/joc

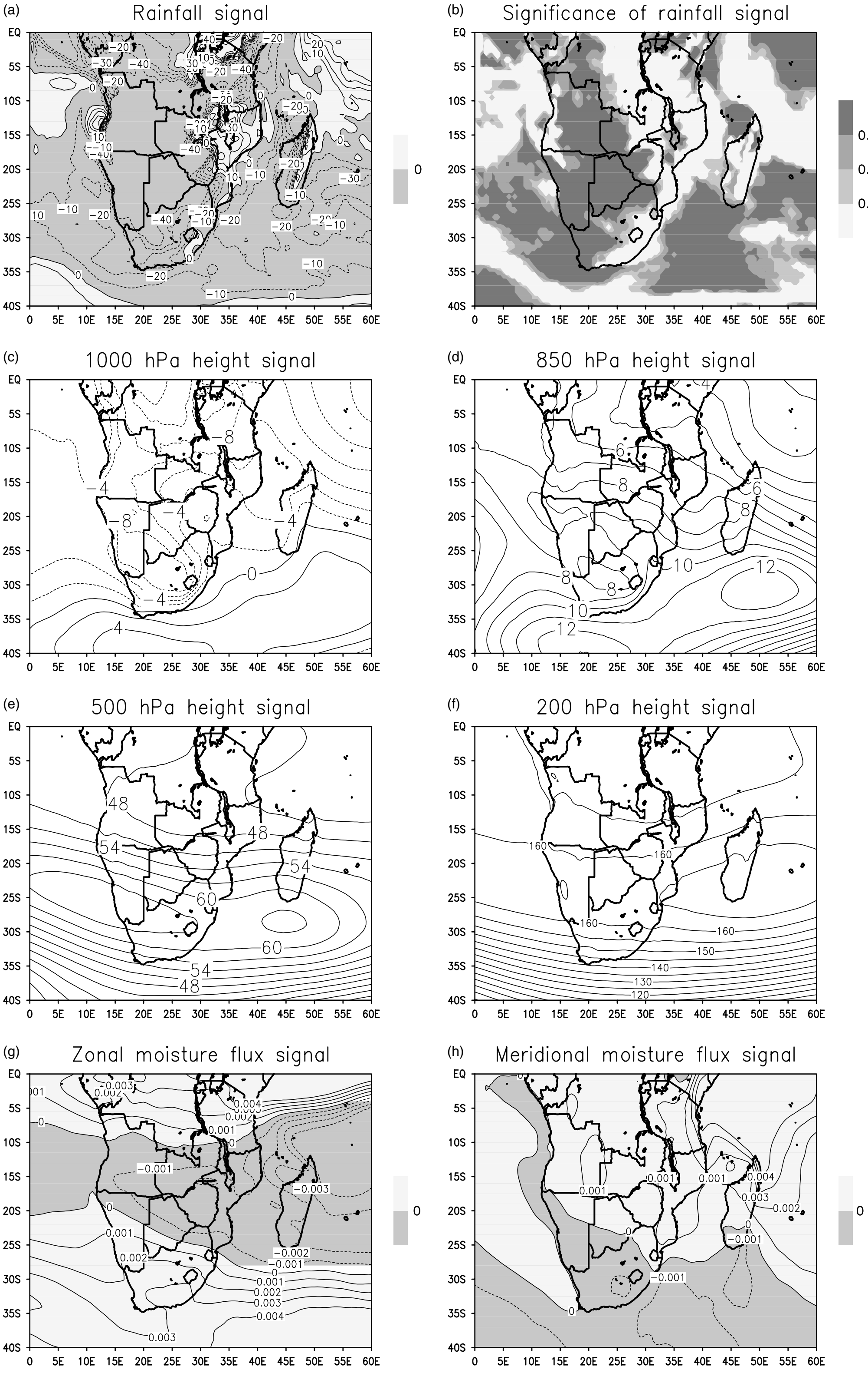

Figure 7. Projected winter (JJA) climate-change signal over the subcontinent. Panel (a) shows the rainfall change (percentage) and panel (b) shows the significance level of the rainfall signal; panels (c)–(f) show the geopotential height change (gpm) at the 1000, 850, 500, and 200 hPa levels, respectively; the change in vertically integrated zonal moisture flux (m s^{-1} kg/kg) is displayed in panel (g) and the change in the vertically integrated meridional moisture flux (m s^{-1} kg/kg) is given in panel (h).

4.1. Winter (JJA) climate-change signal

The subtropical high-pressure belt is simulated to intensify south of the subcontinent at 1000 hPa in the winter of the future climate (Figure 7(c)). However, over the subcontinent the continental trough deepens, particularly over the central interior of South Africa,

DOI: 10.1002/joc

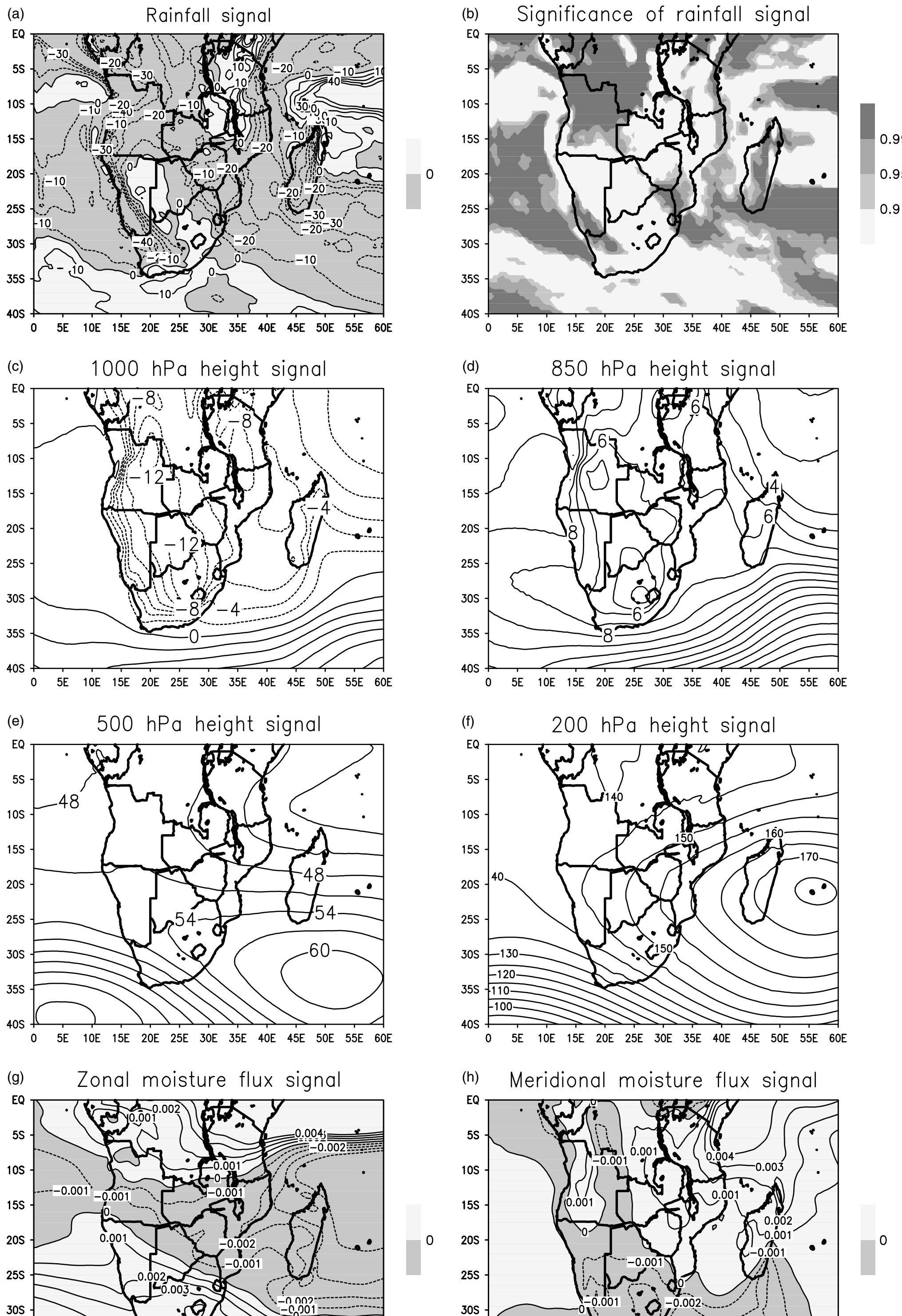

Figure 8. Projected spring (SON) climate-change signal over the subcontinent. Panel (a) shows the rainfall change (percentage) and panel (b) shows the significance level of the rainfall signal; panels (c)–(f) show the geopotential height change (gpm) at the 1000, 850, 500, and 200 hPa levels, respectively; the change in vertically integrated zonal moisture flux (m s^{-1} kg/kg) is displayed in panel (g) and the change in the vertically integrated meridional moisture flux (m s^{-1} kg/kg) is given in panel (h).

Botswana, and Namibia. A similar strengthening of the subtropical high-pressure belt is simulated at 850 hPa (Figure 7d)). In fact, a general increase in geopotential is simulated at this level, but with a minimal increase and a trough-shaped pattern over the western interior of southern Africa. Note that the decreasing 1000 hPa

DOI: 10.1002/joc

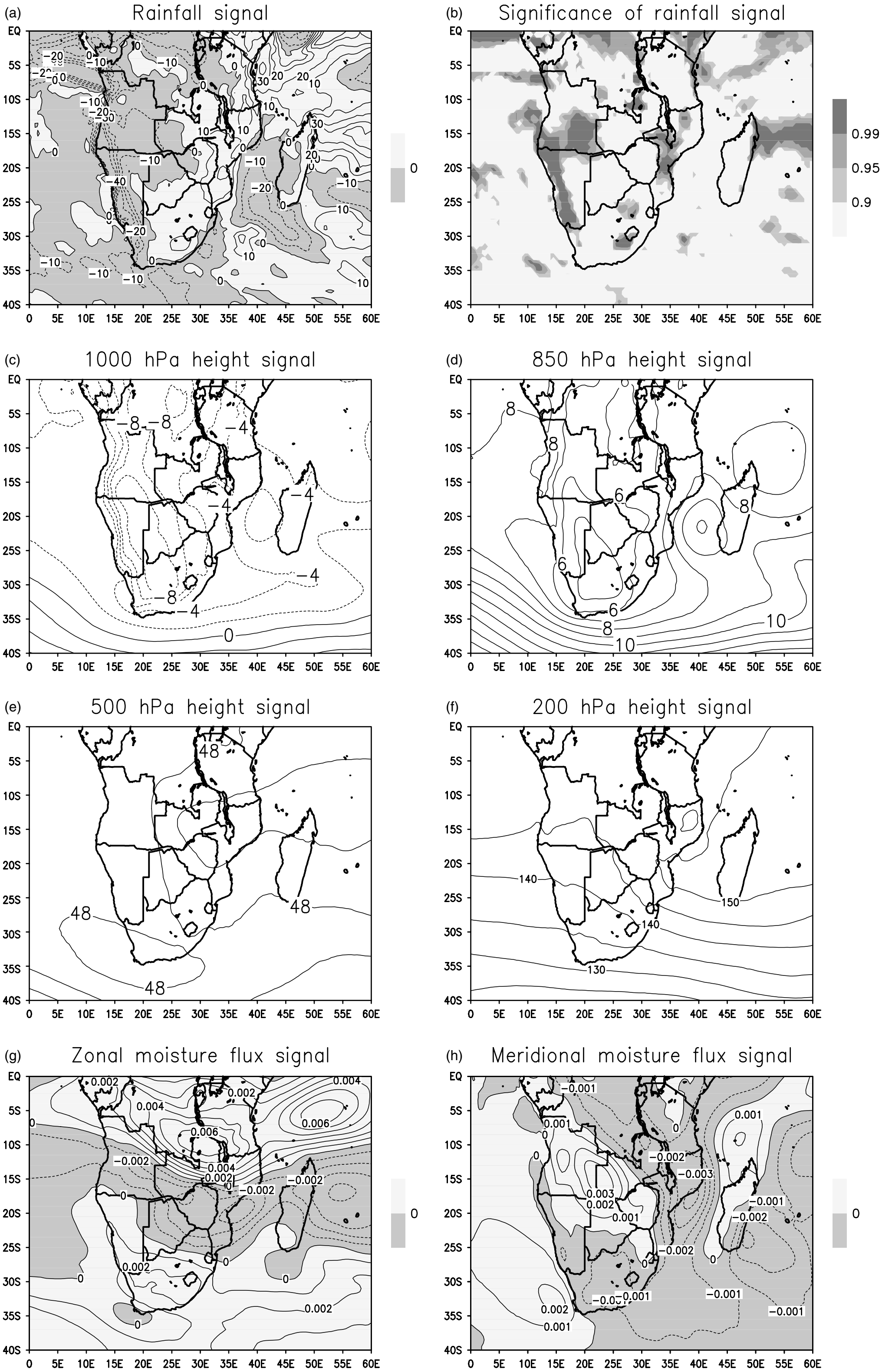

Figure 9. Projected summer (DJF) climate-change signal over the subcontinent. Panel (a) shows the rainfall change (percentage) and panel (b) shows the significance level of the rainfall signal; panels (c)–(f) show the geopotential height change (gpm) at the 1000, 850, 500, and 200 hPa levels, respectively; the change in vertically integrated zonal moisture flux (m s^{-1} kg/kg) is displayed in panel (g) and the change in the vertically integrated meridional moisture flux (m s^{-1} kg/kg) is given in panel (h).

and increasing 850 hPa geopotential anomalies over the western interior are consistent: the 1000 hPa decrease occurs in association with falling surface pressures and higher surface temperatures of the simulated future climate (Engelbrecht, 2005), whilst higher temperatures between the surface and the 850 hPa level lead to

DOI: 10.1002/joc

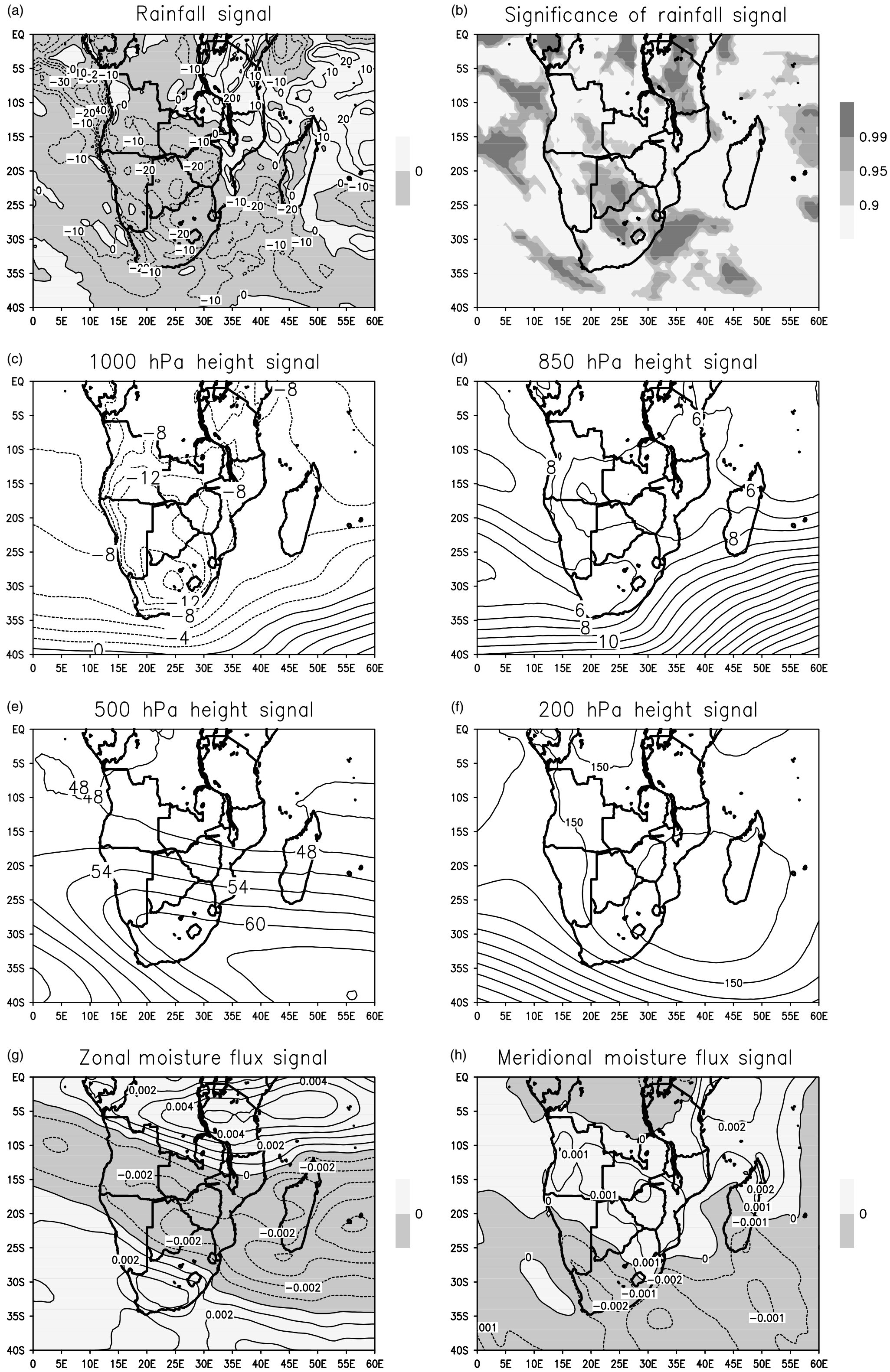

Figure 10. Projected autumn (MAM) climate-change signal over the subcontinent. Panel (a) shows the rainfall change (percentage) and panel (b) shows the significance level of the rainfall signal; panels (c)–(f) show the geopotential height change (gpm) at the 1000, 850, 500, and 200 hPa levels, respectively; the change in vertically integrated zonal moisture flux (m s^{-1} kg/kg) is displayed in panel (g) and the change in the vertically integrated meridional moisture flux (m s^{-1} kg/kg) is given in panel (h).

a rise in the 850 hPa height through the hypsometric relationship. The geopotential height changes at 700 hPa (not shown), 500 hPa and 200 hPa (Figure 7(e) and (f)) reveals that the subtropical high-pressure belt intensifies in the mid and upper levels over southern Africa in winter of the future climate, so that

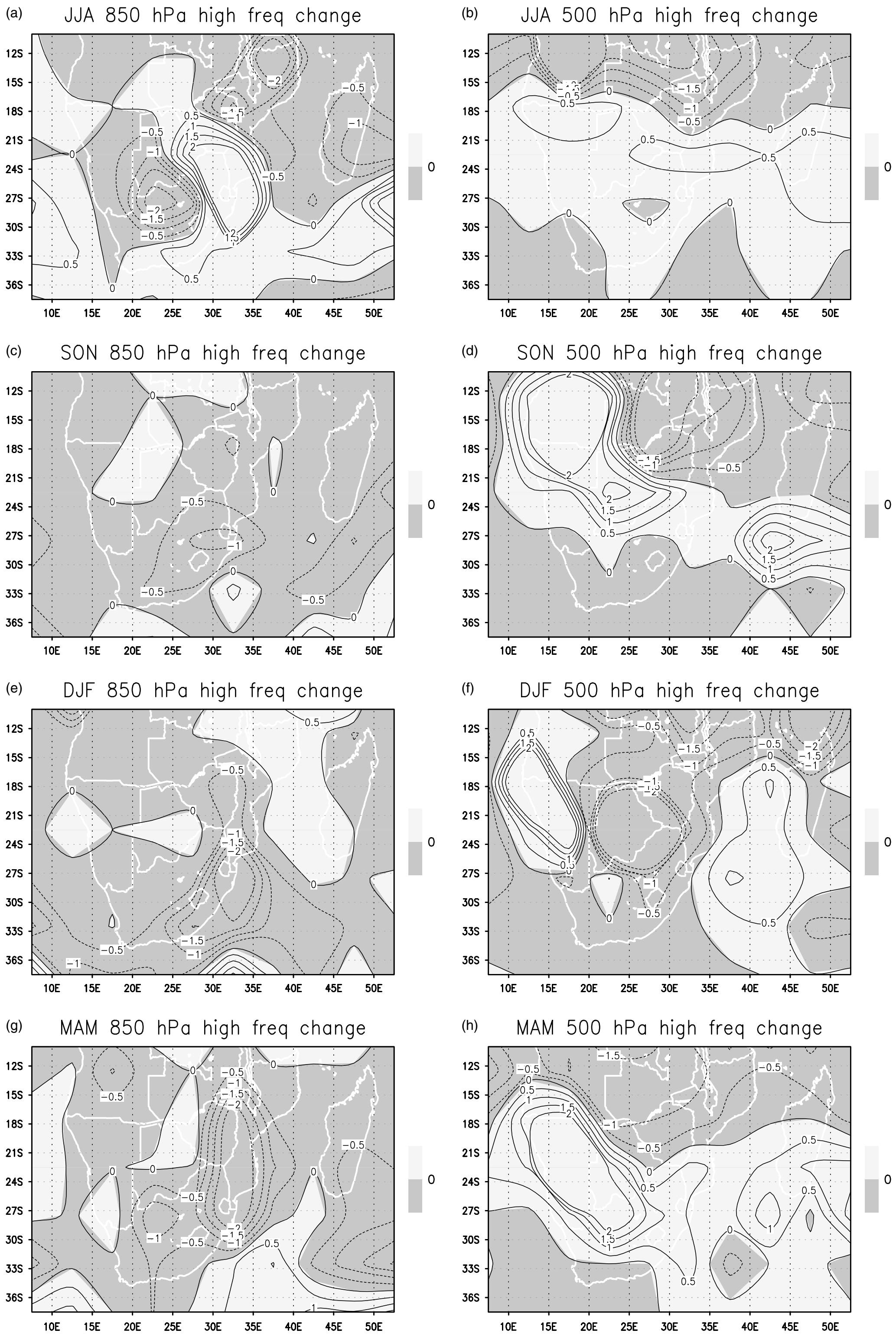

Figure 11. Projected change in the seasonal frequency of local geopotential maxima at 850 and 500 hPa, as calculated over 5° × 5° degree grid boxes at 12-hour intervals. Units are numbers of 12-hour geopotential maxima per season.

the region of maximum intensification is tilted northwards in height with respect to the lower (1000 and 850 hPa) levels.

The more intense subtropical high-pressure belt in the lower levels south of the subcontinent is unfavourable for rainfall over the south-western Cape and Cape south coast. Frontal rain bands are displaced to the south on average, resulting in a decrease (10–40%) in rainfall over the winter rainfall region of the south-western Cape (Figure 7(a)). The projected change is statistically significant at the 99% level (Figure 7(b)). The intensification of the subtropical high between levels 700 and 200 hPa over southern Africa also contributes to conditions unfavourable for winter rainfall, by inducing enhanced zonal flow over the south-western Cape and to the south of the subcontinent (as indicated by the enhanced zonal moisture flux, see Figure 7(g)). Indeed, dry conditions over the south-western Cape are associated with a more intense austral jet south of about 30 °S (Tennant and Reason, 2005). More frequent ridging in the lower levels (Figure 11(a)) is likely to be the reason for the increase in rainfall over the Eastern Cape interior of South Africa and northern Mozambique in the future climate.

4.2. Spring (SON) climate-change signal

The subtropical high-pressure belt is simulated to intensify to the south of the country in the lower levels during SON. The largest intensification is simulated to occur south-east of the subcontinent (Figure 8(c) and (d)), with a northward tilt in height from 850 to 200 hPa over the south-west IO (Figure 8(e) and (f)). The continental trough is simulated to intensify over the western and central interior of the subcontinent at 1000 hPa (Figure 8(c)). Although a general increase in geopotential is simulated for the 850 hPa level, the increase is minimal and displays a trough-shaped pattern over the western and central subcontinent (Figure 8(d)). In fact, with the maximum increase in the geopotential occurring over the IO south-east of the subcontinent, it may be said that a relative deepening of the continental trough occurs at the 850 hPa level of the future climate.

The geopotential anomalies support an increase in anti-cyclonic circulation over the southern part of the IO, and to the west over the eastern and central parts of southern Africa. Indeed, an increase in the frequency of 500 hPa highs is projected over these regions, but also further to the west over northern Namibia and Angola (Figure 11(d)). An enhanced westward moisture flux from the IO into Mozambique and further westward into the central parts of southern Africa is simulated (Figure 8(g)). To the west of the region of maximum increase in geopotential in the mid (700 and 500 hPa) and upper (200 hPa) levels, an enhanced southward flux of moisture is simulated to occur over eastern Namibia, south-western Botswana and the central parts of South Africa (Figure 8(h)). That is, an enhanced anti-cyclonic moisture flux is simulated along the northern and western periphery of the region of maximum mid and upper level geopotential increase (along the western boundary of the region where the frequency of 500 hPa highs is projected to increase). The (relative) deepening of the continental trough in the lower levels would also promote an enhanced northerly moisture flux over the central and western subcontinent. The positive rainfall anomalies signalled for the future climate seem to occur in an anti-cyclonic pattern along the northern and western periphery of the region with maximum increase in geopotential (Figure 8(a)). A prominent feature is the increase in rainfall simulated in a north-west to south-east directed band over eastern Namibia and western Botswana, towards and over central South Africa. Drier conditions (statistically significant at the 99% level, Figure 8(b)) are simulated over eastern Botswana, Zimbabwe, north-eastern South Africa, southern Mozambique and a large portion of the southern IO. This drying occurs underneath the region of maximum increase in geopotential, where stronger subsidence may be expected in association with the enhanced anti-cyclonic circulation (e.g. Preston-Whyte and Tyson, 1988).

It may be noted that the band of positive rainfall anomalies simulated over southern Africa seems to be linked with a similar north-west to south-east directed band over the IO south of the subcontinent. Simultaneously, a similarly directed band of negative rainfall anomalies is simulated to occur to the north-east over the IO, originating over the south-eastern subcontinent and also covering much of Madagascar. Rainfall variability over southern Africa and the south-west IO is often associated with such a dipole pattern of anomalously wet (dry) conditions over southern Africa concurring with anomalously dry (wet) conditions over the south-west IO (e.g. Tyson, 1986; Washington and Todd, 1999). There is evidence that this dipole pattern is the result of shifts in the South Indian Convergence Zone (SICZ) (Washington and Todd, 1999). The latter is a land-based convergence zone (LBCZ) which has been proposed to originate over the subcontinent where easterly flow from the Indian Ocean High (IOH) converges with flow around the continental trough (e.g. Cook, 2000). It seems as if the model projects the more frequent formation of the SICZ over the central interior of southern Africa, at the expense of its formation over the IO. The deepening of the continental trough over the central interior, in combination with the projected anomalies in geopotential and high frequency, would indeed favour moisture convergence and southward moisture advection over the western to central interior of southern Africa.

4.3. Summer (DJF) climate-change signal

The subtropical high-pressure belt at 1000 hPa in DJF of the future climate (Figure 9(c)) is simulated to intensify further to the south of the subcontinent than in JJA and SON. This may be interpreted as a southern expansion of the subtropical high-pressure belt in the future climate, or alternatively, as a widening of the tropical belt (see Seidel *et al.*, 2008). Although there is a general decrease in geopotential over the IO at 1000 hPa, a prominent ridge-like pattern is present over and to the east of Madagascar, suggesting a more prominent IOH in the future climate. Indeed, more frequent low-level ridging is projected for the Mozambique Channel and Madagascar (Figure 11(e)). Simultaneously the continental trough is simulated to deepen, and relatively large negative geopotential anomalies are simulated to extend from the south-eastern coastal areas of the subcontinent into the south-western IO. At 850 hPa a similar pattern is present (Figure 9(d)). The subtropical high-pressure belt strengthens to the south of the country with the IOH strengthening over the IO east of Madagascar and to

DOI: 10.1002/joc

the west over Madagascar into the Mozambique Channel. That geopotential gradient between the continental trough and the IOH tightens. The 700 hPa geopotential signal (not shown) is very similar to the 850 hPa signal. The 500 hPa signal is also similar, although in this case the maximum strengthening of the IOH is simulated to occur somewhat to the south compared to the 700 and 850 hPa patterns (Figure 9(e)). However, at 200 hPa the geopotential signal differs considerably from that at lower levels, with the maximum positive anomalies located over the IO to the north of Madagascar (Figure 9(f)).

Consistent with the described geopotential changes, the more frequent formation of mid-level highs is projected over the IO to the east of South Africa (Figure 11(f)). Simultaneously, the frequency of trough formation over southern Africa is projected to increase (not shown). These changes, together with the intensification of the IOH in the lower levels and the broad deepening of the continental trough, would promote moisture convergence and the more frequent formation of the SICZ over southern Mozambique and eastern South Africa (e.g. Cook, 2000). Indeed, anomalously high rainfall is projected to occur in a band stretching from southern Mozambique and eastern South Africa into the IO, with a band of anomalously low rainfall present to the north-east (Figure 9(a)). This suggests a westward shift of the SICZ from its typical position (e.g. Washington and Todd, 1999; Cook, 2000). Note that these changes occur in relation to enhanced southward moisture advection over the IO (Figure 9(h)), to the west and south of the more intense IOH. However, the projected rainfall changes are slight and statistically significant only over parts of eastern South Africa (Figure 9(b)).

The western subcontinent is simulated to become significantly drier in DJF. Another prominent feature of the DJF rainfall signal is the wetter conditions (generally significant at the 95% significance level) simulated east of northern Madagascar and over Mozambique (Figure 9(a) and (b)). These rainfall anomalies are associated with an enhanced westward moisture flux over the IO, westwards over northern Madagascar and into Mozambique (Figure 9(g)), that occurs to the north of the more intense IOH. Negative geopotential anomalies are projected to occur at 1000 hPa over the IO in the future climate (Figure 9(c)), with an associated increase in geopotential and the more frequent formation (not shown) of highs at 200 hPa over the same region (Figure 9(f)). This circulation structure would favour the development of tropical systems over the northern IO. Indeed, an increase in the frequency of 850 hPa lows is projected over northern Madagascar (not shown). The possible increase in the frequency of tropical depressions (including tropical cyclones) over this part of the IO is an important aspect of climate change over southern Africa that remains to be investigated rigorously (Christensen *et al.*, 2007).

4.4. Autumn (MAM) climate-change signal

A deepening of the continental trough at 1000 hPa and the displacement of the subtropical high-pressure belt to the south of the subcontinent is simulated for MAM, similar to the DJF signal (Figure 10(c)). However, the high-pressure belt is simulated to intensify more prominently over the south-western IO to the south-east of South Africa. At 850 hPa the maximum intensification of the subtropical high-pressure belt also occurs south-east of the subcontinent over the south-western IO (Figure 10(d)). Similar to the SON geopotential height signal, the region of maximum intensification of the high-pressure belt is tilted northwards with height from 850 to 200 hPa (Figure 10(e) and (f)). However, in the mid levels the positive geopotential anomalies from the IO extend further to the west over the subcontinent in autumn compared to spring. Indeed, the more frequent formation of highs over the central and western parts of southern Africa at 500 hPa is projected (Figure 11(h)).

The result of this increase in mid and upper level geopotential over southern Africa is enhanced mid-level subsidence (Preston-Whyte and Tyson, 1988), which causes much of southern Africa to become drier in the future climate. A strong decrease (significant at the 99% level) in MAM rainfall is simulated to occur in a band stretching from north-eastern Namibia over Botswana to eastern South Africa. This change suggests that cloud-band formation over the region will occur less frequently in the future climate, as a result of the dominant effect of the more frequently occurring mid-level highs. A moderate increase in rainfall is signalled for Mozambique, with a statistically significant increase projected for Tanzania. The former increase occurs in conjunction with enhanced westward moisture advection that occurs to the north of the stronger IOH (Figure 10(g)). Moisture advection around stronger mid-level highs (note the enhanced southward moisture flux over southern Namibia and the western interior of South Africa in Figure 10(h)), in conjunction with the more intense continental trough in the lower levels (Figure 10(c) and (d)), is the likely mechanism responsible for the slight increase in rainfall simulated over southern Namibia and the western interior of South Africa (Figure 10(a)).

4.5. Annual climate-change signal

Figure 12 shows the percentage change in yearly rainfall, under current and future forcings. Over large portions of the subcontinent the projected change is relatively small, in the order of 10% or less, and statistically insignificant. Thus, although relatively larger changes are projected for specific seasons, some of the seasonal effects cancel each other resulting in relatively small changes in annual rainfall. Over South Africa the south-western Cape is projected to become significantly drier with a rainfall decrease of about 20%. This decrease is linked to the southward displacement of frontal rain bands during winter as noted earlier; indeed the yearly rainfall is projected to increase over the ocean to the south of the subcontinent. Although wetter conditions are projected over eastern South Africa during DJF of the future climate, Figure 12 illustrates that yearly rainfall is projected

DOI: 10.1002/joc

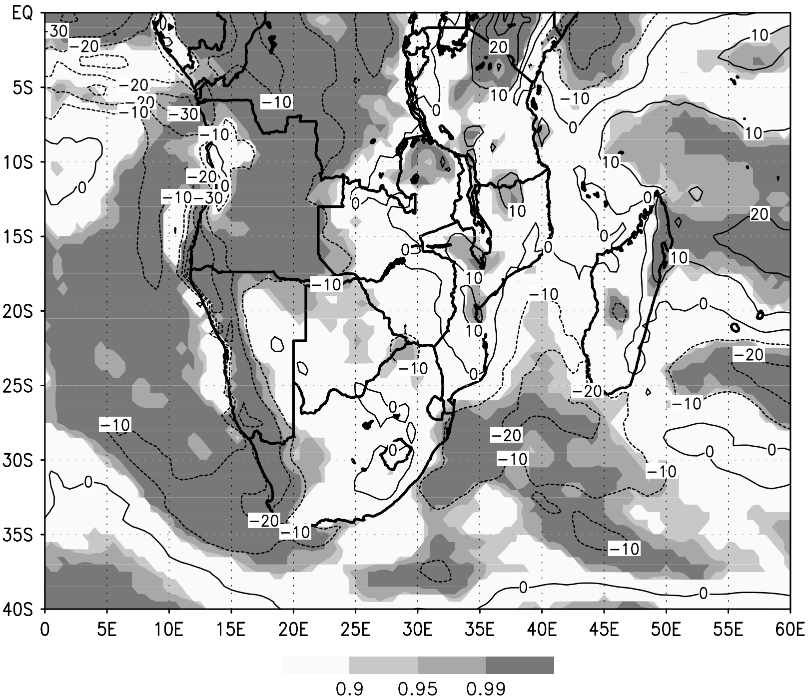

Figure 12. Percentage change in yearly rainfall under current and future forcings. Shading indicates the statistical significance.

to decrease over this region. The decrease is statistically significant over the north-eastern parts of the country. Thus, the subsidence and drier conditions associated with the more frequent occurrence or intensification of mid and upper level highs over this region during SON and MAM dominate over the DJF projected increase in rainfall. In fact, the only part of South Africa where an increase in yearly rainfall is projected is the central interior. This increase may possibly be linked to enhanced cloud-band formation over the region during SON and DJF, as described earlier, but is statistically insignificant. The model projection of a generally drier South Africa, with an increase in rainfall over the central interior, is in contrast to the perception that South Africa will become wetter in the east and drier in the west (e.g. DEAT, 2006). It may also be noted that in a recent study of observed rainfall tendencies over South Africa, an increase in rainfall was noted over the central interior of the country with negative tendencies present over the eastern interior (Kruger, 2006). The generally wetter conditions over northern Mozambique may be linked to the general increase in the westward moisture flux over this region, that occurs to the north of a more intense subtropical high-pressure belt. Much of the western subcontinent is projected to become generally drier in the future climate, with statistically significant decreases in rainfall of between 10 and 30% noted for large portions of Namibia, Botswana, Angola, and the DRC.

5. Summary and conclusions

A variable-resolution GCM, CCAM, has been used to simulate present-day (1975–2005) and future (2070–2100) climate at high horizontal resolution over southern and tropical Africa. The A2 SRES scenario was used to describe the anthropogenic forcing, with SSTs described from a fully coupled (1871–2100) simulation of the CSIRO Mk3.0 OAGCM. A number of shortcomings in the model simulation of present-day rainfall and circulation have been identified, but in general the model provides a satisfactory description of the intra-annual rainfall cycle over the subcontinent. In particular, the model managed to correctly simulate that over southern Africa the regions with highest monthly rainfall percentages follow an anti-cyclonic path in time, starting over the east coast of South Africa in September and then subsequently being displaced to north-eastern South Africa, Zimbabwe, southern Zambia, northern Botswana and Namibia, eventually reaching southern Namibia and the western interior of South Africa in March (e.g. Taljaard, 1986).

The model-projected rainfall climate-change signal may to a large extent be interpreted in terms of projected changes in the location and intensity of the subtropical high-pressure belt and the IOH in particular. In winter the subtropical high-pressure belt is simulated to intensify to the south of the subcontinent in the lower troposphere, with the region of maximum intensification being tilted northward with height in the mid and upper levels over southern Africa. These changes induce enhanced zonal flow over South Africa and a displacement of frontal rain bands towards the south, which are unfavourable for rainfall over the winter rainfall region of South Africa (Tennant and Reason, 2005). Indeed, a considerable and statistically significant decrease in rainfall over the winter rainfall regions of South Africa is projected for the future climate. During spring of the future climate

DOI: 10.1002/joc

the low-level continental trough is projected to deepen over the western interior of the subcontinent, whilst the IOH strengthens in the mid and upper levels over the IO and the eastern and central parts of southern Africa. This pattern favours cloud-band formation over the central interior of South Africa, that is, the more frequent occurrence of the SICZ over this region, as opposed to its occurrence over the south-western IO (e.g. Washington and Todd, 1999; Cook, 2000). During summer of the future climate the continental trough deepens broadly over the subcontinent, a feature which may be interpreted as an expanding tropical belt (e.g. Seidel *et al.*, 2008). The IOH intensifies over the south-western IO and Madagascar in the lower and mid levels. Much of eastern southern Africa is projected to become wetter in summer, as the circulation changes favour the formation of the SICZ over the south-eastern subcontinent, opposed to its occurrence to the north-east over the south-western IO and southern Madagascar (e.g. Washington and Todd, 1999; Cook, 2000). To the north of the more intense IOH much of Mozambique is projected to become wetter in enhanced easterly flow. In fact, a pattern of decreasing low-level geopotential is projected over the northern IO with an associated increase in upper level geopotential. This pattern favours the occurrence of tropical depressions over the IO, which would then travel westwards into Mozambique in the enhanced easterly flow. In autumn the intensification of the continental trough is projected to be most prominent over the western subcontinent, similar to the projected spring pattern. More intense (or more frequently occurring) mid and upper level highs are projected to dominate the circulation over southern Africa. A general decrease in rainfall is projected over southern Africa in association with the enhanced subsidence underneath the highs (e.g. Preston–Whyte and Tyson, 1988). Only over the far western parts of the region, along the western periphery of these highs, is a slight increase in rainfall projected for autumn.

The yearly rainfall totals show little change in the future climate, with changes generally projected to be less than 10%. An important exception is the south-western Cape of South Africa, where a considerable decrease in rainfall is projected. Eastern South Africa is projected to become drier despite the projected increase in summer rainfall. This is in contrast to the general perception that South Africa will become wetter in the east and drier in the west as a result of greenhouse gas forcing e.g. (DEAT, 2006). The central interior of South Africa is the only part of the country that is projected to become wetter in the future climate. Interestingly, some observed trends in climate correspond to the model projection of future climate: the tropical belt has been observed to expand over the last three decades (e.g. Seidel *et al.*, 2008), whilst observed rainfall tendencies over South Africa indicate an increase in rainfall over central South Africa with negative tendencies over the eastern interior (Kruger, 2006).

The projected spring to autumn future rainfall patterns over southern Africa have been linked to the main present-day mode of rainfall variability over the region, namely shifts in the location of the SICZ. Similarly, the projected winter rainfall change has been linked to a sound dynamic forcing mechanism. The projected intensification of the subtropical high-pressure belt and IOH (and associated changes in the SICZ) may in turn be fundamentally linked to the deepening of the continental trough and increased convection in the tropics, as induced by the enhanced greenhouse effect. The deeper continental trough and increased convection in the tropics would ultimately induce enhanced subsidence over the IO and to the south of the subcontinent, strengthening the subtropical high-pressure belt and the IOH in particular (e.g. Engelbrecht, 2004). Thus, from a dynamic circulation perspective the projection may be considered as a plausible scenario of climate change over southern Africa. However, it should be noted that the climate-change projection presented is one of only a few similar RCM studies performed over southern Africa (e.g. Arnell *et al.*, 2003; Tadross *et al.*, 2005; Olwoch *et al.*, 2007). It represents only a single outcome of possible future climate change over the region. There is a need to perform more regional climate-change modelling studies over Africa, for different SRES scenarios using different models, in order to obtain a broader view of the range of potential future climate change over the subcontinent (e.g. Hulme *et al.*, 2005; Christensen *et al.*, 2007). Continuous high-resolution simulations, for say 1871–2100, may provide additional insight into how climate change may evolve over southern Africa. For example, it has been proposed that in the late-summer climate of southern Africa, cloud-band formation may progressively be displaced westwards as mid-level highs become more and more prominent over eastern southern Africa (Engelbrecht, 2004). Finally, analysis of observed upper-air sounding data and reanalysis data may reveal if circulation changes over southern Africa, such as a shift in the preferred location of the SICZ, have indeed already occurred as a result of anthropogenic forcing.

Acknowledgements

The authors would like to thank Dr Fourie Joubert of the Bioinformatics and Computational Biology Unit at the University of Pretoria for making available the computer cluster that was used to perform the climate simulations described in the study. The research formed part of a project sponsored by the Water Research Commission in South Africa. Comments by Prof Willem A. Landman and two anonymous reviewers have helped to improve the paper.

References

Arnell NW, Hudson DA, Jones RG. 2003. Climate change scenarios from a regional climate model: estimating change in runoff in southern Africa. *Journal of Geophysical Research* **108**(D16): 4519, Doi:10.1029/2002JD002782.

Basher R, Briceno S. 2005. Global warming and African climate change: a reassessment. In *Climate Change and Africa*, Low PS (ed.). Cambridge University Press: Cambridge, Chapter 25; 271–283.

Battisti DS. 1995. Decadal to Century time-scale variability in the coupled Atmosphere-ocean: modelling issues. *Natural Climate Variability on Decade-to-century Time Scales*. National Research Council, National Academy Press, Washington D.C.; 419–429.

Christensen JH, Hewitson B, Busuioc A, Chen A, Gao X, Held I, Jones R, Kolli RK, Kwon W-T, Laprise R, Magana Rueda V, Mearns L, Menendez CG, Raisanen J, Rinke A, Sarr A, Whetton P. 2007. Regional climate projections. In *Climate Change 2007: The Physical Science Basis. Contribution of Working Group I to the Fourth Assessment Report of the Inter-governmental Panel on Climate Change*, Solomon S, Qin D, Manning M, Chen Z, Marquis M, Averyt AB, Tignor M, Miller HL (eds). Cambridge University Press: Cambridge, New York.

Cook KH. 2000. The South Indian convergence zone and interannual rainfall variability over southern Africa. *Journal of Climate* **13**: 3789–3804.

Department of Environmental Affairs and Tourism (DEAT). 2006. South Africa environment outlook. *A Report on the State of the Environment*. Department of Environmental Affairs and Tourism: Pretoria; 371.

Deque MP, Marquet P, Jones RG. 1998. Simulation of climate change over Europe using a global variable resolution general circulation model. *Climate Dynamics* **14**: 173–189.

Engelbrecht FA. 2004. The new climate of Southern Africa. In *Proceedings of the 20th Annual Conference of the South African Society for Atmospheric Sciences*, Cape Town, May 2004.

Engelbrecht FA. 2005. Simulations of climate and climate change over Southern and tropical Africa with the conformal-cubic atmospheric model. In *Climate Change and Water Resources in Southern Africa: Studies on Scenarios, Impacts, Vulnerabilities and Adaptation*, Schulze RE (ed.). Water Research Commission: Pretoria, RSA, WRC Report 1430/1/05, Chapter 4; 57–74.

Engelbrecht FA, Rautenbach CJdeW, McGregor JL, Katzfey JJ. 2002. January and July climate simulations over the SADC region using the limited-area model DARLAM. *Water SA* **28**: 361–374.

Gordon HB, Rotstayn LD, McGregor JL, Dix MR, Kowalczyk EA, O'Farrell SP, Waterman LJ, Hirst AC, Wilson SG, Collier MA, Watterson IG, Elliott TI. 2002. *The CSIRO Mk3 Climate System Model*. CSIRO Atmospheric Research: Australia; 130.

Hewitson BC, Crane RG. 2006. Consensus between GCM climate change projections with empirical downscaling. *International Journal of Climatology* **26**: 1315–1337.

Hulme M, Doherty R, Ngara T, New M. 2005. Global warming and African climate change: a reassessment. In *Climate Change and Africa*, Low PS (ed.). Cambridge University Press: Cambridge; Chapter 3; 29–40.

Hope PK, Nicholls N, McGregor JL. 2004. The rainfall response to permanent inland water in Australia. *Australian Meteorological Magazine* **53**: 251–262.

Joubert AM, Katzfey JJ, McGregor JL, Nguyen KC. 1999. Simulating mid-summer climate over southern Africa using a nested regional climate model. *Journal of Geophysical Research* **104**: 19015–19025.

Kalnay E, Kanamitsu M, Kistler R, Collins W, Deaven D, Gandin L, Iredell M, Saha S, White G, Woollen J, Zhu Y, Chelliah M, Ebisuzaki W, Higgins W, Janowiak J, Mo KC, Ropelewski C, Wang J, Leetmaa A, Reynolds R, Jenne R, Joseph D. 1996. The NCEP/NCAR 40-year reanalysis project. *Bulletin of the American Meteorological Society* **77**: 437–472.

Kruger AC. 2006. Observed trends in daily precipitation indices in South Africa: 1910–2004. *International Journal of Climatology* **26**: 2275–2286.

Lal M, McGregor JL, Nguyen KC. 2008. Very high resolution climate simulation over Fiji using a global variable-resolution model. *Climate Dynamics* **30**: 293–305.

McGregor JL. 1996. Semi-Lagrangian advection on conformal-cubic grids. *Monthly Weather Review* **124**: 1311–1322.

McGregor JL. 1997. Regional climate modelling. *Meteorology and Atmospheric Physics* **63**: 105–117.

McGregor JL. 2005a. Geostrophic adjustment for reversibly staggered grids. *Monthly Weather Review* **133**: 1119–1128.

McGregor JL. 2005b. C-CAM: Geometric aspects and dynamical formulation. CSIRO Atmospheric Research Technical Paper, No 70, 41.

McGregor JL, Dix MR. 2001. The CSIRO conformal-cubic atmospheric GCM. In *IUTAM Symposium on Advances in Mathematical Modelling of Atmosphere and Ocean Dynamics*, Hodnett PF (ed.). Kluwer: Dordrecht; 197–202.

McGregor JL, Nguyen KC, Katzfey JJ. 2002. Regional climate simulations using a stretched-grid global model. In *Research Activities in Atmospheric and Oceanic Modelling Report No. 32*, Ritchie H (ed.). Geneva; WMO/TD-No. 1105, 3.15–3.16.

McGregor JL, Walsh K. 1994. Climate change simulations of Tasmanian precipitation using multiple nesting. *Journal of Geophysical Research* **99**: 20889–20905.

Meadows ME. 2006. Global change and southern Africa. *Geographical Research* **44**: 135–145.

New M, Hulme M, Jones P. 1999. Representing twentieth-century spacetime climate variability. Part I: development of a 1961–90 mean monthly terrestrial climatology. *Journal of Climate* **12**: 829–856.

Nunez M, McGregor JL. 2007. Modelling future water environments of Tasmania, Australia. *Climate Research* **34**: 25–37.

Olwoch JM, Reyers B, Engelbrecht FA, Erasmus BFN. 2007. Climate change and the tick-borne disease, Theileriosis (East Coast fever) in sub-Saharan Africa. *Journal of Arid Environments* **72**: 108–120.

Preston-Whyte RA, Tyson PD. 1988. *The Atmosphere and Weather of Southern Africa*. Oxford University Press: Cape Town; 374.

Reason CJC, Rouault M. 2002. ENSO-like decadal variability and South African rainfall. *Geophysical Research Letters* **29**(13): 1638, No 10.1029/2002 GL014663.

Renwick JA, Katzfey JJ, McGregor JL, Nguyen KC. 1999. On regional model simulations of climate change over New Zealand. *Weather and Climate* **19**: 3–14.

Rotstayn LD. 1997. A physically based scheme for the treatment of stratiform clouds and precipitation in large-scale models. I: Description and evaluation of the microphysical processes. *Quarterly Journal of the Royal Meteorological Society* **123**: 1227–1282.

Schulze RE, Lumsden TG, Horan MJC, Warburton M, Maharaj M. 2005. An assessment of impacts of climate change on agrohydrological responses over southern Africa. In *Climate Change and Water Resources in Southern Africa: Studies on Scenarios, Impacts, Vulnerabilities and Adaptation*, Schulze RE (ed.). Water Research Commission: Pretoria, RSA WRC Report 1430/1/05. Chapter 9; 141–189.

Schwarzkopf MD, Fels SB. 1991. The simplified exchange method revisited: an accurate, rapid method for computation of infrared cooling rates and fluxes. *Journal of Geophysical Research* **96**: 9075–9096.

Seidel DJ, Fu Q, Randel WJ, Reichler TJ. 2008. Widening of the tropical belt in a changing climate. *Nature Geoscience* **1**: 21–24.

Sushama L, Laprise R, Caya D, Frigon A, Slivitzky M. 2006. Canadian RCM projected climate-change signal and its sensitivity to model errors. *International Journal of Climatology* **26**: 2141–2159.

Tadross M, Jack C, Hewitson B. 2005. On RCM-based projections of change in southern African summer climate. *Geophysical Research Letters* **32**: L23713, DOI:10.1029/2005GL024460.

Taljaard JJ. 1967. Development, distribution and movement of cyclones and anticyclones in the Southern Hemisphere during the IGY. *Notos* **14**: 73–84.

Taljaard JJ. 1986. Change of rainfall distribution and circulation patterns over southern African summer. *International Journal of Climatology* **6**: 579–592.

Taljaard JJ. 1996. Atmospheric circulation systems, synoptic climatology and weather phenomena of South Africa. Part 6. Rainfall in South Africa. *Technical Paper* no 32, SA Weather Bureau, Pretoria.

Tennant WJ, Reason CJC. 2005. Associations between the global energy cycle and regional rainfall in South Africa and Southwest Australia. *Journal of Climate* **18**: 3032–3047.

Tyson PD. 1986. *Climate Change and Variability in Southern Africa*. Oxford University Press: Cape Town; 220.

Walsh K, McGregor JL. 1995. January and July climate simulations over the Australian region using a limited-area model. *Journal of Climate* **8**: 2387–2403.

Wang Y, Leung LR, McGregor JL, Lee D-K, Wang W-C, Ding Y, Kimura F. 2004. Regional climate modeling: progress, challenges, and prospects. *Journal of the Meteorological Society of Japan* **82**: 1599–1628.

Washington R, Todd M. 1999. Tropical-temperate links in southern African and southwest Indian Ocean satellite-derived daily rainfall. *International Journal of Climatology* **19**: 1601–1616.

Whetton PH, Katzfey JJ, Hennessy KJ, Wu X, McGregor JL, Nguyen KC. 2001. Developing scenarios of climate change for Southeastern Australia: an example using regional climate model output. *Climate Research* **16**: 181–201.